Oxygen Vacancies and Hydrogen in Amorphous In-Ga-Zn-O and ZnO

Hongfei Li[1], Yuzheng Guo[1,2], John Robertson[1],

1 Engineering Department, Cambridge University, Cambridge CB2 1PZ, UK
2 School of Engineering, University of Swansea, Swansea, SA1 8EN, UK

Abstract

Hydrogen is known to be present as an impurity in amorphous oxide semiconductors at the 0.1% level. The behavior of hydrogen and oxygen vacancies in amorphous In-Ga-Zn-O is studied using density functional supercell calculations. We show that the hydrogens pair up at oxygen vacancies in the amorphous network, where they form metal-H-metal bridge bonds. These bonds are shown to create filled defect gap states lying just above the valence band edge, infra-red modes at about 1400 and 1520 cm^{-1}, and they are shown to give a consistent mechanism to explain the negative bias illumination stress instability found in oxide semiconductors like In-Ga-Zn-O (IGZO).

Introduction

Amorphous oxide semiconductors such as InGaZn oxide (IGZO) are replacing hydrogenated amorphous silicon (a-Si:H) as the main large-area semiconductor for display applications for both drivers of organic light emitting diodes, and for pixel switches in active matrix liquid crystal displays, because of their higher electron mobility [1,2]. The high mobility of these oxides arises from the s-like character of their conduction band edge states, which are less sensitive to disorder [1-4]. Roughly speaking, for IGZO, the In supplies the mobility, the Zn makes the system amorphous by the mixed ion effect and Ga helps to make oxygen deficiency more costly.

However, despite these advantages, IGZO suffers from some instabilities, particularly the negative bias illumination stress (NBIS) instability [5-10], whose mechanism is still contentious. The instability is essentially a persistent photoconductivity caused by the photo-excitation of electrons from defect gap states lying just above the valence band edge into the conduction band. The gap states are seen by hard x-ray photoemission spectroscopy (XPS) [11,12].

The have been several models for this effect, but each model has problems. The instability has been linked by many groups to the oxygen vacancy because the vacancy is a common defect in oxides, and the instability tends to be worse in oxygen deficient samples [13-17]. The O vacancy is also a 'negative U' defect, which produces an energy barrier which inhibits the recombination of the photo-excited electrons and so gives rise to the persistent photoconductivity [18,19]. However the vacancy states lie too high in the gap compared to their energy as seen by photoemission.

Another possibility is that the instability is due to oxygen interstitials, which have been seen in various random network models, and which, unlike vacancies, give rise to states in the right energy range just above the valence band edge [20-24]. This defect can also have a negative U property in some cases. However, the interstitial is an oxygen excess defect, and processing the films to remove oxygen deficiency is known to reduce the instability [16,17].

The third possibility is that the instability is due to hydrogen [25-26]. It has been proposed that the instability is due to single hydrogen atoms undergoing a deep to shallow transition and becoming a donor, and thereby creating the photoconductivity. However, this model also does not correspond to an oxygen deficiency. On the other hand, annealing IGZO in water vapor at certain temperatures or in low levels of hydrogen can reduce the number of active defects [27,28]. Generally, hydrogen and water have some unusual behaviors in these oxides and this would benefit from a deeper understanding [29-32]. Hydrogen bond to oxygen sites without some other defect cannot be the cause of NBIS as the O-H group only produces states below the valence band, as shown later.

We have recently proposed that the instability is caused by a hydrogen atom pair at an oxygen vacancy, based on calculations using amorphous (a-) ZnO as a simple model system [33]. This model is an adaption of the defect in c-ZnO previously studied by Du and Biswas [34]. The hydrogen pair were shown to give rise to filled states in the lower part of the band gap of ZnO, just where they are observed by XPS in a-IGZO [11]. The infra-red signature of bridging metal-H bonds, a key aspect of

the hydrogen atom pair defect, has also been observed at about 1400 and 1520 cm^{-1} by Bang et al [35]. The defect is an oxygen deficient defect and also has the negative U property.

However, hydrogen has a range of behaviors in crystalline ZnO, for example as an interstitial donor [36-40] but generally hydrogen has a lower concentration in crystalline ZnO than the carrier concentration seen in the photo-excited state of a-IGZO, or the density of gap states seen in photoemission. Also, ZnO is not readily made amorphous [41], so it is also useful to study the defect behavior in amorphous IGZO itself.

Thus, it would be useful to show that the hydrogen pair model applies to a-IGZO itself, to show why the amorphous IGZO or a-ZnO can absorb more hydrogen than the crystalline oxides, and to show why the hydrogen tends to exist as the compensated state not as the donor state when present in larger quantities. To do this, we study the oxygen vacancy in c-ZnO, a-ZnO and IGZO, to find its dependence on disorder, and on composition in IGZO. We then calculate the properties of two hydrogens at the O vacancy, and how this defect formation energy varies with disorder, and how it varies from ZnO to IGZO. Overall, it is found that disorder lowers the cost of creating the O vacancy, and this allows higher H concentrations. It is also found that hydrogen in higher concentrations as in the amorphous phase tends to pair up into a compensated state. Thus, hydrogen in amorphous IGZO tends to follow Anderson's model that an electron-lattice coupling tends to open up a band gap at the Fermi level, which overcomes any doping effects.

Methods

The calculations of defect geometries are carried out using the ab-initio plane-wave density-functional code CASTEP [42]. We use norm-conserving pseudopotentials, retaining the Zn 3d, 4s and O 2s, 2p orbitals in the valence shell. Initially, the generalized gradient approximation (GGA) is used to represent the electronic exchange-correlation function. Energy minimization continues until the residual force on each atom is below 0.001eV/Å. The simple GGA grossly under-estimates the band gap in the post-transition metal oxides like ZnO [43-46]. The GGA+U method is used to improve this. It applies an empirical repulsive potential U to both the Zn 3d states and O 2p states to widen the gap [43-45]. It has a similar computational cost as GGA itself, and it is used in this paper for molecular dynamics calculations to generate random network structures and for relaxing large supercell models. However, it does not fully open up the gap, and it is less reliable for the hydrogen states.

Thus for the electronic spectra and total energy calculations such as for defect formation energies, we use the screened exchange hybrid functional [47]. This is a parameter-free functional which mixes in a fraction of exact (Hartree-Fock) exchange with the local density approximation exchange-correlation functional, screened as a function of distance. It gives the correct band gaps, but is over x100 slower than GGA.

Another hybrid functional, by Heyd, Scuseria and Ernzerhof (HSE) [48], is also used in some cases to calculate defect formation energies in the random networks. In this case, the fraction of Hartree-Fock exchange is increased from the standard value of 25% up to 37.5% in order to fit the ZnO band gap, following Oba [49]. However, this version does slightly under-estimate the binding energies of the Zn 3d states compared to experiment [50].

The defect formation energies of the intrinsic defects are calculated within the scheme of Lany and Zunger [51] to correct for finite size effects for the charged defects. The formation energies of each charge state are given by

$$H_q(E_F,\mu) = [E_q - E_H] + q(E_v+\Delta E_F) + \sum_\alpha n_\alpha(\mu_\alpha^0 +\Delta\mu_\alpha) \qquad [1]$$

where q is the charge on the system, E_q is the energy of charged system with a defect, E_H is the energy of charged system with no defect. E_V is the valence band maximum (VBM) and E_F is the Fermi level with the respect to VBM. n_α is the number of atoms of species α, μ_α is the relative chemical potential of element α. We note that the first two terms are equal to the difference between the total energy of charged defect system and total energy of the neutral defect-free system. Oba et al [49] have cpreviously studied the finite size effects for ZnO and noted that 96 atom supercells are enough to allow for corrections.

Generally, defect formation energies are quoted at the thermodynamic equilibrium limits, such as O-rich given by the O chemical of the O_2 molecule, or the O-poor limit given by the Zn/ZnO

equilibrium. In the Zn-O-H system, this is complicated because the H_2/H_2O equilibrium is in the same energy range, so that the relevant limit here is the O-poor/H-rich limit [34].

Results

Bulk ZnO

Fig. 1(a) shows the band structure of bulk crystalline wurzite ZnO calculated by the sX functional. The calculated band gap is 3.4 eV, which equals the experimental value. The Zn 3d states lie at -7.7 eV [50]. The calculated heat of formation is -3.87 eV per O atom.

The amorphous ZnO models of 96 atoms were built in several stages. First, a random network of ZnO is created by a high temperature molecular dynamics (MD) anneal of crystalline ZnO at 2000 K for 20 ps. It is then cooled down to 300 K in 20 ps. Finally, the system is relaxed to an energy minimum.

The density of a-ZnO is set at 4.62 g/cm^3 compared to 5.44 g/cm^3 for c-ZnO [52]. The heat of formation of a-ZnO is calculated to be -3.28 eV per O atom in HSE compared to 3.87 eV per O atom for c-ZnO (Table 1). The density of a-ZnO has a considerable effect on its heat of formation, and also, as we see shortly, on the formation energy of its O vacancies.

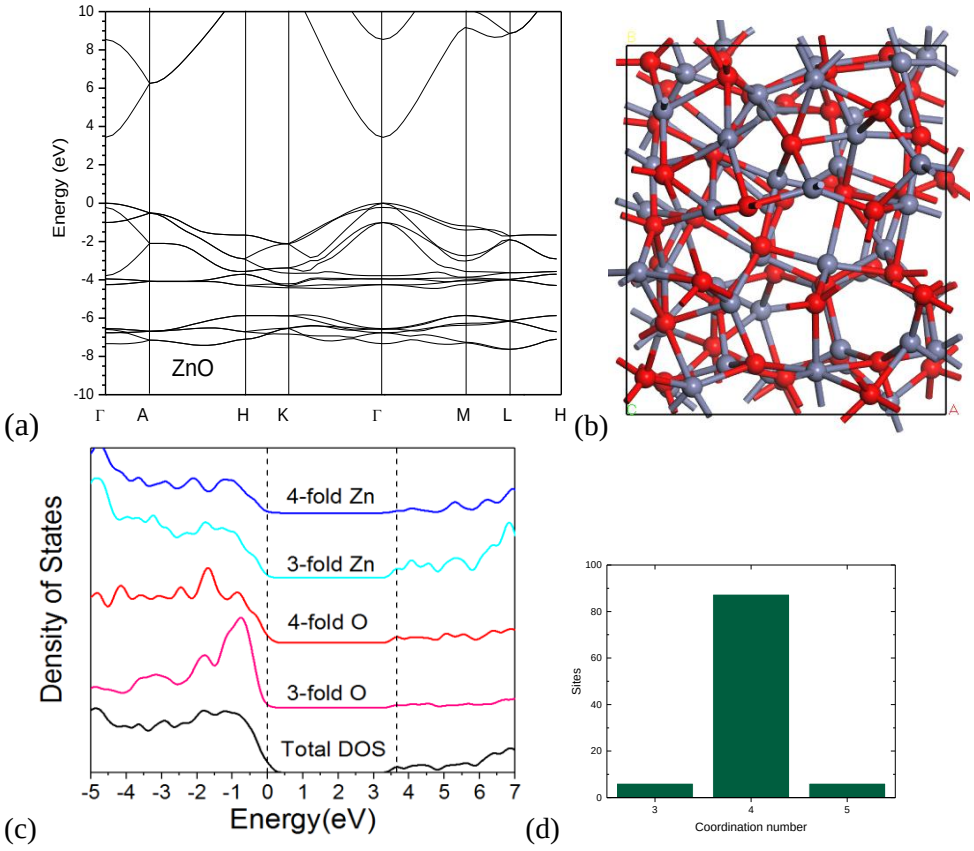

Fig. 1. (a) Band structure of wurzite ZnO using the sX functional. (b) An amorphous ZnO random network, (c) the partial density of states on the bulk 4-fold and 3-fold Zn and O sites compared. (grey = Zn, red = O) and (d) its coordination number distribution.

ZnO is basically a sp^3 bonded network. It can be compared to the random networks of III-V compounds like a-GaAs. Unlike a-GaAs, a-ZnO is a fully chemically ordered network with no like-atom bond, Fig 1(b) [53]. As in a-GaAs, the other possible defect in a-ZnO is the mis-coordinated atom for example 3-fold Zn or 3-fold O. This type of defect was recognized early on in a-GaAs [54,55]. In previous calculations on the III-V network a-AlN, the fraction of 3-fold sites depended on the basis set [56,57], but this is less of a problem when a plane wave basis set is used.

Fig. 1(b) shows one of the calculated a-ZnO random networks. The presence of a bond between adjacent atoms was analyzed using the bond overlap population rather than in terms of bond distances. The bond overlap integral is the overlap integral of the occupied plane-wave states projected onto localized orbitals on atomic sites, S=<a|b>. A cut-off at S=0.05 is used to define whether a bond exists or not. The coordination distribution is shown in Fig. 1(d). We find there are no like-atom bonds in the network, and that there are under 3% of 3-fold or 5-fold Zn and O sites.

Fig 1(c) shows the partial density of states (PDOS) on the 4-fold and 3-fold Zn and O sites of the random network. We see that the states of the 'defect' 3-fold sites lie around the band edges of the majority 4-fold sites, but they do not form states within the band gap. In this sense, they could be considered to be like 3-fold sites on a non-polar (110) surface of c-ZnO.

Bulk c- and a-IGZO

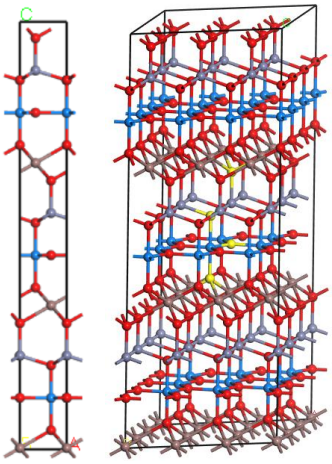

Fig 2. (a) unit cell of c-IGZO. (b) The four different O vacancy sites in c-IGZO, shown in yellow. (red = O, grey = Zn, blue = Ga, brown = In).

Fig 2(a) shows the unit cell of crystalline IGZO [58,59,60]. The unit cell is long and thin, which is less convenient for supercell calculations. Each metal atom has a different coordination, Zn is 4-fold tetrahedral, Indium is 6-fold octahedral, while Ga has a 5-fold coordinated site with 3 bonds within a plane and two apical sites along Oz. The oxygen sites are a mixture of 4-fold and 3-fold coordination. The structure has features of a layered structure with Ga-O bonds almost forming a plane on which is built a layer of tetrahedral Zn sites with oxygens, followed by the octahedrally coordinated In sites.

(a)

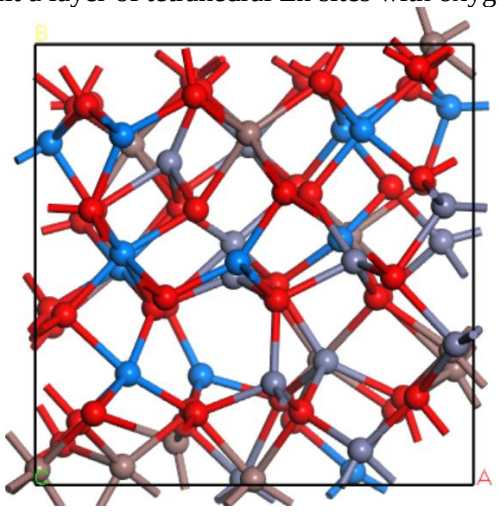

(b)

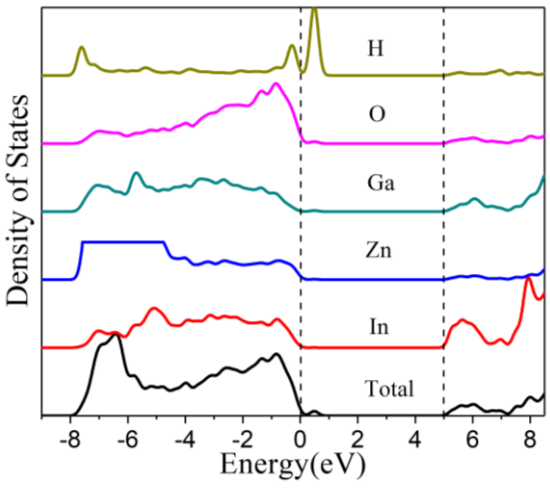

Fig. 3. (a) Random network of a-IGZO: with blue=Ga, brown=In, grey=Zn, red=O. (b) the partial density of states (PDOS) of each atom type, including at a H bridge site. The Zn 3d PDOS is cut-off at the top.

Fig 3(a) shows a 116 atom random network of a-IGZO. The density of a-IGZO is taken as 6.04 g/cm^3 compared to 6.36-6.4 g/cm^3 for the crystalline phase, from experiment [61,62,23]. In this network, most Zn atoms have 4-fold coordination and most In and Ga are 5-fold or 6-fold coordinated as in other works [59,60,23]. There are only metal-oxygen bonds. Fig 3(b) gives the PDOS of crystalline IGZO for sX. The band gap is 3.1 eV.

The heat of formation of crystalline IGZO can be calculated to be -3.91 eV per O atom in HSE with α=0.375%. This heat of formation is very close to that of ZnO. This arises because In_2O_3 has lower heat of formation per O, but Ga_2O_3 has a higher heat of formation than ZnO.

The heat of formation of a-IGZO is -3.60 eV per O atom in HSE, compared to -3.91 eV per O atom for the crystal. This is a smaller change on amorphization for IGZO than for ZnO, showing that IGZO can be amorphized more easily. This is expected for a three cation system.

	crystalline	amorphous
ZnO	-3.87 (5.44 g/cm^3)	-3.28 (4.62 g/cm^3)
Ga2O3	-4.21	
In2O3	-3.92	
IGZO	-3.91 (6.4 g/cm^3)	-3.60 (6.04 g/cm^3)
H2O	-3.34	
H2	-4.09	

Table 1. Calculated heats of formation per O atom (eV), from HSE with mixing fraction α=0.375. Mass densities for each phase are also given.

O vacancies in ZnO

There is a single type of O vacancy in ZnO, where the vacancy site is surrounded by four Zn atoms, each with a Zn sp^3 hybrid directed to the vacancy [19]. In c-ZnO, the vacancy formation energy is calculated to be 4.62 eV in the O-rich limit and 1.28 eV in the O-poor limit.

Normally, the vacancy formation energy is calculated in the O-rich limit (where the O chemical potential is half that of the O_2 molecule) and in the O-poor limit (where the O chemical potential is that of the metal oxide/metal equilibrium.) However, for the case of oxides containing hydrogen, the O-poor limit can be defined instead as that of the H_2/H_2O equilibrium which lies at -3.34 eV, just below that of the Zn/ZnO equilibrium.

Oxygen vacancy	Formation energy (eV/O)		
	O rich	O poor (H_2/H_2O equil)	$V_O/2H^0$ O-poor
Vo (xtal)	4.62	1.28	1.97
Vo1	0.96	-2.32	-0.15
Vo2	1.08	-2.21	0.23
Vo3	2.40	-0.88	-2.51
Vo4	2.82	-0.46	-0.28
Vo5	2.88	-0.40	-1.35
Vo6	3.79	0.51	-3.43
Vo7	4.19	0.91	1.16

Table 2. Formation energies of 7 representative O vacancies in a-ZnO compared to a vacancy in c-ZnO. Note the large range. Also given are the formation energies of the neutral $V_O/2H$ complexes in

c-ZnO and a-ZnO in the O-poor/H-rich limit. The energy of this complex in the O-rich limit is 6.57 eV larger.

In a-ZnO, we have examined 7 representative oxygen vacancies. These are found to cover a wide range of formation energies, from 0.96 eV to 4.19 eV in the O-rich limit, or -2.32 eV to 0.91 eV in the O-poor limit (Table 2). These defect formation energies are a large change from those in c-ZnO. Fundamentally, this occurs because of the lower density of a-ZnO and also because of the relative instability of a-ZnO compared to c-ZnO. This means that the O vacancy and the surrounding network can relax its atomic configuration considerably in a-ZnO and so reduce its formation energy.

O vacancies in IGZO

Turning to IGZO, there are four chemically distinct types of O vacancy sites in crystalline IGZO, as shown in yellow in Fig. 2(b) and enlarged in Fig 4. Table 3 shows their defect formation energies in the O-rich and O-poor limits as calculated in HSE (α=0.375). The formation energy varies with the vacancy, according to the types of bond broken to form the vacancy [63]. To rationalize this, we have given the bond strengths an empirical 'composition index' of 1 for Ga-O, 0.5 for Zn-O and -1 for In-O. The formation energies are found to vary roughly in proportion to this index, see Fig 6.

We have then created 8 representative oxygen vacancies in a-InGaZnO. These are found to have a range of formation energies, as given in Table 4. Again, the vacancy formation energy depends primarily on the type of bonds broken to form the vacancy, as in the crystal. We plot in Fig 6 the vacancy formation energy in the O-poor limit in a-IGZO against this index. It is seen to give a good description of the variation, showing that chemical disorder is the main component of the formation energy rather than the structural disorder.

It is particularly noticeable that the range of defect formation energies for O vacancies in a-IGZO (1.4 eV) is much smaller than that in a-ZnO (3 eV) and much closer to their formation energy in the crystal. This indicates that IGZO is able to tolerate disorder more easily than a-ZnO. Also a-IGZO is 5.96% less dense than c-IGZO where a-ZnO is 17.7% less dense than c-ZnO.

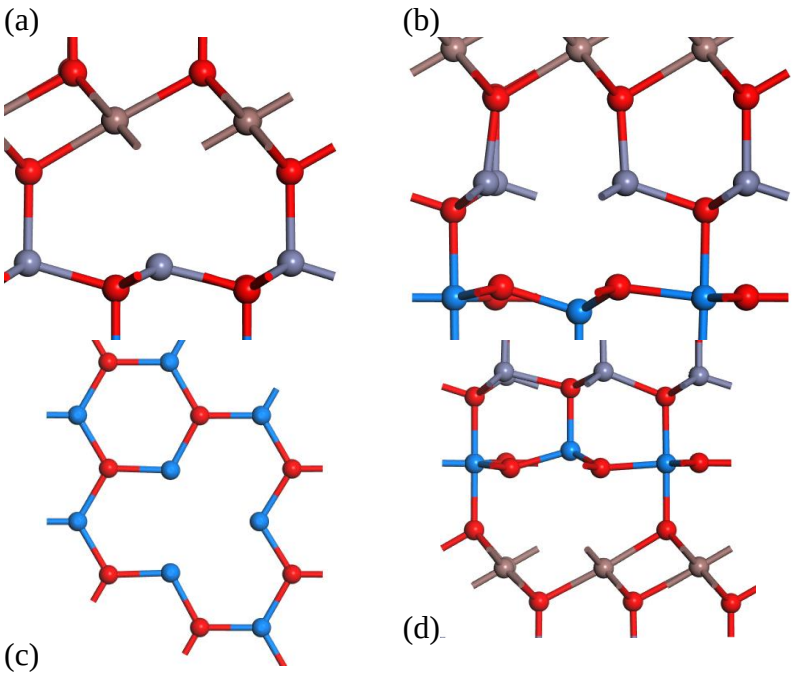

Fig. 4. The coordinations of the four chemically different O vacancy sites in c-IGZO.

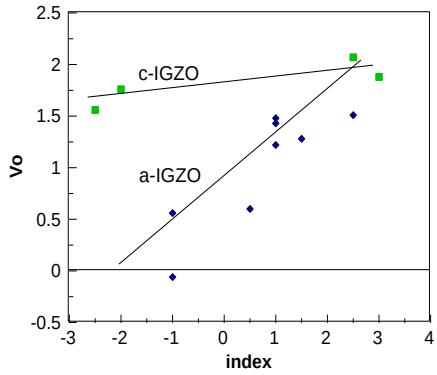

Fig. 5. Formation energy for various O vacancies in c-IGZO and a-IGZO vs. an empirical 'compositional index' as given in Tables 3 and 4.

	Formation energy (eV/O)			Number of neighbors			
Oxygen vacancy	O rich	O poor (H_2/H_2O equil)	$V_O/2H^0$ O-poor/ H-rich limit	In	Ga	Zn	index
Vo1	4.90	1.56	2.57	3	0	1	-0.5
Vo2	5.41	2.07	2.49	0	1	3	2.5
Vo3	5.21	1.88	2.26	0	3	0	3
Vo4	5.10	1.76	3.09	3	1	0	-2

Table 3. Vacancy formation energy in the O-poor limit (HSE α=0.375) and the type of metal neighbors for different O vacancies for c-IGZO. Also given is the formation for the neutral $V_O/2H$ complex.

	Formation energy (eV)			Number of neighbors			
Oxygen vacancy	O rich	O poor (H_2/H_2O equil)	$V_O/2H^0$, O-poor limit	In	Ga	Zn	index
Vo1	4.62	1.28	1.66	1	2	1	1.5
Vo2	4.56	1.22	1.57	1	1	2	1
Vo3	3.94	0.60	0.76	1	0	3	0.5
Vo4	4.81	1.48	1.91	1	1	2	1
Vo5	4.85	1.51	-0.12	0	1	3	2.5
Vo6	4.77	1.43	2.25	1	1	2	1
Vo7	3.89	0.56	1.07	2	1	0	-1
Vo8	3.28	-0.06	1.62	2	1	0	-1

Table 4. Vacancy formation energy in the O-poor and O-rich limit, and the number of metal neighbors for various O vacancy configurations in a-IGZO. Also given is the formation energy for the neutral $V_O/2H$ complex.

Hydrogen configurations at c-ZnO defects and surfaces

We now discuss hydrogen bonding configurations, first in ZnO and then in IGZO. As a reference system, the hydrogen bonding in silicon is easily described. Si has four sp^3 hybrids each possessing one electron. When a Si sp^3 hybrid bonds to a hydrogen, each atom contributes one electron to the Si-H electron-pair bond.

In ZnO, the Zn-O bond is also a 2-electron bond. However these are polar, with Zn contributing only ½ electron and O contributing 3/2 electron. This still allows filled bonding states to be formed as long as there are only Zn-O bonds. Electron counting has a profound effect on the possible bonding configuration of hydrogen, as it does in other systems, following Pashley and others [64,65]. At the O vacancy, the missing O means that the four Zn sp^3 hybrids pointing into the vacancy have only ½

electron each. When these try to bond to hydrogen, this leaves 3/2 electrons for a Zn-H bond and 2.5 electrons for a O-H bond. Specifically, they would not be able to form four filled Zn-H bonds at the vacancy. Pairs of configurations are formed to avoid these fractional electrons.

Table 5. Electron count for various bonding configurations in ZnO.

Bond	Electron count	Total count
Zn-O	½ + 3/2	2
Zn-H	½ + 1	1.5
≡Zn-H-Zn≡	½ + 1 + ½	2
≡Zn-O-H	3/2 + 1	2.5

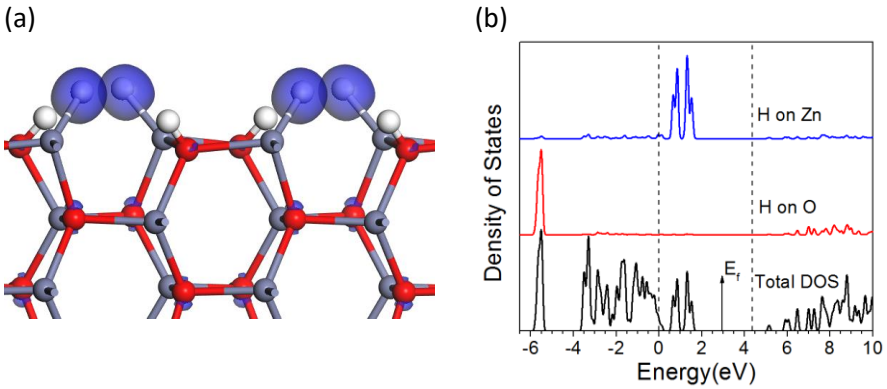

Fig. 6. A non-polar ZnO(110) surface with both O-H and Zn-H groups. A PDOS for monovalent OH and ZnH groups.

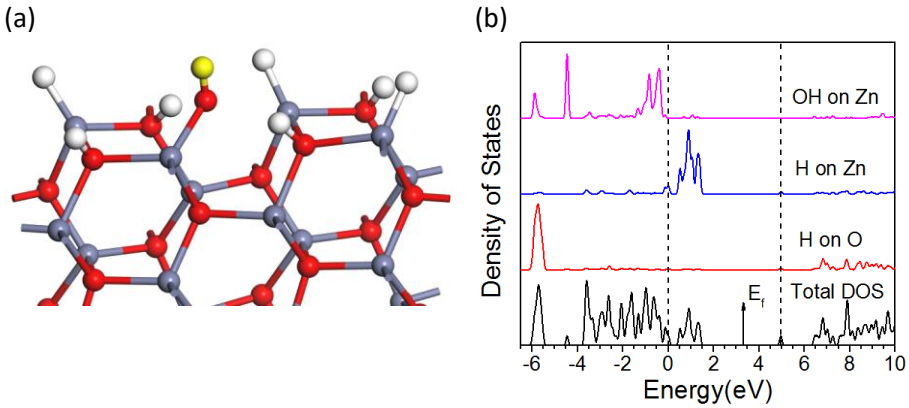

Fig. 7. A ZnO(110) surface with –O-H, Zn-H and Zn-OH groups, and (b) their PDOS. The top of the bulk valence band is set to 0 eV.

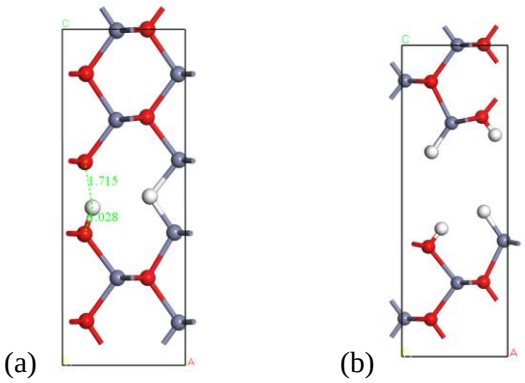

Fig. 8. Energy comparison between (a) Zn-H and (b) Zn-H-Zn structure. Formation Energy is 0.58eV for (a), and 0.95eV for (b).

The bonding possibilities must the satisfy 'electron counting rules', to give a completed valence shell and a Fermi energy lying in midgap. We consider this by referring to species attached to the non-polar (110) surface of cubic ZnO. The (110) surface has alternating Zn and O dangling bonds on each surface atom [63]. Fig. 6(a) shows the (110)ZnO surface with hydrogens attached to the surface Zn and O sites to make Zn-H and O-H units. This combination has a completed valence shell. Fig. 6(b) shows the PDOS of the various groups where the Zn-H bond gives rise to filled Zn-H states at +0.5 eV and +1.5 eV above the valence band edge (there are two states because the surface unit cell has two Zn-H units). The Zn-H bond length is 1.54Å. The orbital shown in Fig 6(a) is the 1.5 eV state. There is also a filled bonding state at -5.0 eV at the bottom of the valence band. The O-H group gives a filled state at -5.8 eV. Here the O is back-bonded to three Zn sites.

Fig. 7(a) shows this surface where one of the surface Zn-H groups is replaced by a monovalent –OH group bonded to a Zn site. Here, the O-H bond gives rise to a filled state at -6.0 eV in Fig 7(b).

Figs 6(b), 7(b) show that O-H groups, as occurring at a hydrogenated Zn vacancy, would only produce states in the lower valence band and not in the gap, and so they cannot be the origin of the NBIS effect.

Fig. 8(a) shows the creation of a Zn-H-Zn bridge bond embedded on a (100)ZnO surface. The (100) surface is polar, but the system can be made charge-balanced by removing 50% of the surface oxygens and substituting a H as an Zn-H-Zn bridge for this O, and by putting an H on top of the other surface oxygen site. In the PDOS in Fig. 8(b) the Zn-H-Zn bridge gives a state at +1.0 eV and at -6.0 eV, which is similar to that of Zn-H-Zn group at the $(V_O/2H)^0$ vacancy complex. The Zn-H bond length in this case is 1.63 – 1.69 Å. The purpose of these various calculations is to give confidence in our calculated energy levels in more complicated systems such as –ZnO:H or hydrogenated vacancies.

Finally, we calculate the relative stability of the terminal Zn-H and bridging Zn-H-Zn groups. This is done for the reaction in Fig. 8, giving that the Zn-H-Zn group is more stable than the terminal Zn-H group by 0.37 eV. Thus although in principle single Zn-H bonds can form, energetically the Zn-H-Zn bridge is slightly more stable.

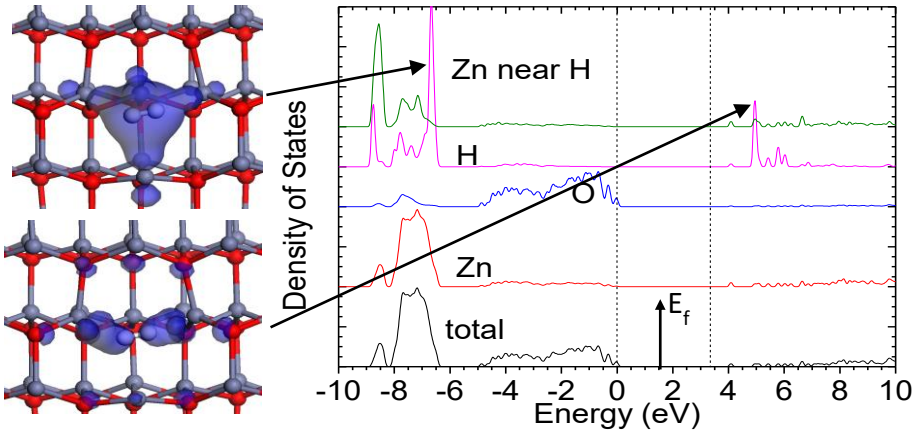

Fig. 9(left). The H_2 molecular unit in the O vacancy V_O^{2+} in ZnO. (right) the PDOS of H and Zn sites at the defect. The orbital charge densities of the states at -7.2 eV and +4.8 eV are shown on the left.

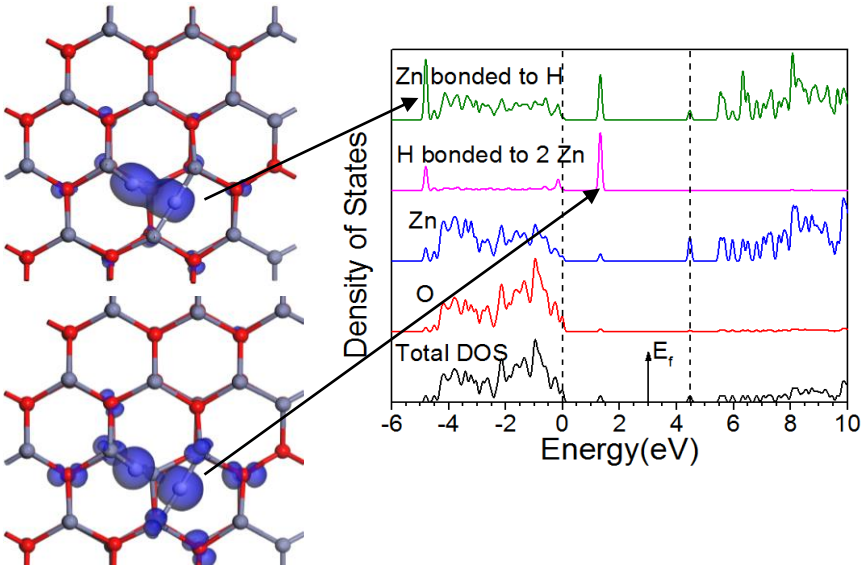

Fig. 10(left). The configuration of $V_O(2H)^0$ with bridging Zn-H-Zn groups. (right) PDOS of the H and adjacent Zn sites. The charge density of the filled orbitals at -5 eV and +1.0 eV are given on the left.

We now consider some behavior of hydrogen at defects in c-ZnO, before passing onto a-ZnO and a-IGZO. Fig. 9 shows the calculated structure of the hydrogen atom pair at the oxygen vacancy in its 2+ state, $(V_O/2H)^{2+}$. In this case, the four Zn sp^3 hybrids are all empty, and the two hydrogens use their two electrons to form a H_2 molecule within the V^{2+} vacancy. The H_2 bonds within itself, and it forms essentially no bonds to the surrounding Zn sites, because the sp^3 hybrids are empty. Fig. 4(b) shows the partial density of states (PDOS) spectrum on the H site and on the adjacent Zn sites, and for the bulk Zn, O sites for reference. The H_2 molecule forms two states, a filled bonding state at -7.2 eV and an empty anti-bonding state at 4.8 eV in the conduction band. Fig. 9(left) shows the charge density of these two states, bonding at -7.2 eV and antibonding +4.8 eV. Their orbital characters are consistent with these assignments.

Fig. 10(left) shows the calculated structure of the neutral complex $(V_O/2H)^0$. Here, the hydrogen atoms are separated and each forms a Zn-H-Zn bridge bond to two adjacent Zn sites of the O vacancy. Fig 10(right) shows the PDOS on the H site and on the adjacent Zn sites. We see that there are filled localized states on H lying at -5.0 eV, and a filled state on the H and Zn sites lying in the gap at +1.5 eV. Fig. 10(left) shows the charge density for the state at -5.0 eV. Overall, the charge density is strongly localized on the hydrogen which is in fact an anion, H^-, so the defect is $V_O^{2+}/2H^-$ overall. Fig 10 also shows the charge density for the filled state at +1.5 eV.

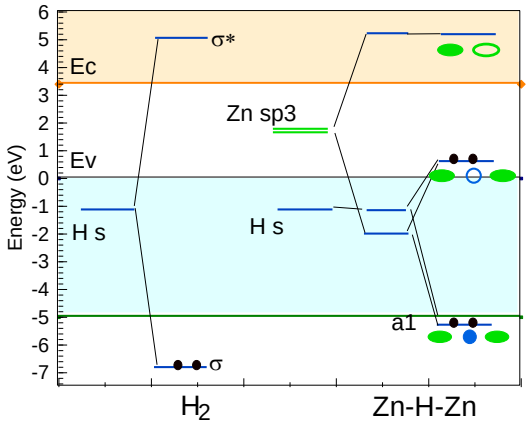

Fig. 11 Schematic molecular orbital diagram of the V_O/2H complex in ZnO, in (a) the +2 and (b) the neutral charge state.

We can analyze the bonding in the bridging configurations using a defect molecule of three local orbitals, the |s> state on the hydrogen and two Zn sp^3 hybrids, $|Zn_1>$ and $|Zn_2>$, as in Fig. 11. For the $(V_O/2H)^{2+}$ case where the H_2 molecule forms, and for the bulk valence band maximum lying at 0 eV, we obtain that the H 1s orbital lies at E_H = -1.2 eV, and the two-center H-H interaction is V_{HH} = -6.0 eV. The overall energy levels are shown on the left of Fig. 11. For the neutral $(V_O/2H)^0$ case, the two hydrogens in the vacancy form two separate Zn-H-Zn bridges with a 3-center bond. The orbitals form three states as on the right of Fig 11. The Zn states form a symmetric combination $|+> = (1/\sqrt{2})(|Zn_1> + |Zn_2>)$ and an anti-symmetric combination $|-> = (1/\sqrt{2})(|Zn_1> - |Zn_2>)$. The |+> state interacts with |s> to form the bonding combination at -5.5 eV and a *filled* anti-bonding combination in the gap at +1.3 eV. This leaves an *empty* |-> state lying at +5 eV in the conduction band. Overall, the hydrogen |s> state is essentially 100% filled because of 50% contributions from each of the -5.5 eV and +1.3 eV states. This enables us to assign the empty state at ~5 eV as the |-> state which was difficult from the PDOS, due to its broadening by resonance with the conduction band.

	eV
E(Zn sp^3)	1.5
E(H)	-1.2
V(Zn-H)	-2.05
V(Zn-Zn)	-4.3
V(H-H), in H_2	-6.0

Table 5. Orbital interactions in defect molecule model of the V_O/2H complex in its +2 and neutral charge states.

The Zn sp^3 state lies at roughly E_{Zn} = +1.5 eV, the Zn-Zn interaction is given by $V_{Zn,Zn}$ = -4.3 eV and the Zn-H interaction is $V_{Zn,H}$ = -2.05 eV. It is notable that the Zn sp^3 state energy is not compatible with the higher Zn,p energy derived when fitting the bulk ZnO band structure as in Kobayashi et al [66]. Note that, overall, the vacancy complex has two bridges with C_{2v} symmetry, but once in the amorphous network, the individual Zn-H-Zn bridges can separate and their states can be analyzed individually, as in Fig 11.

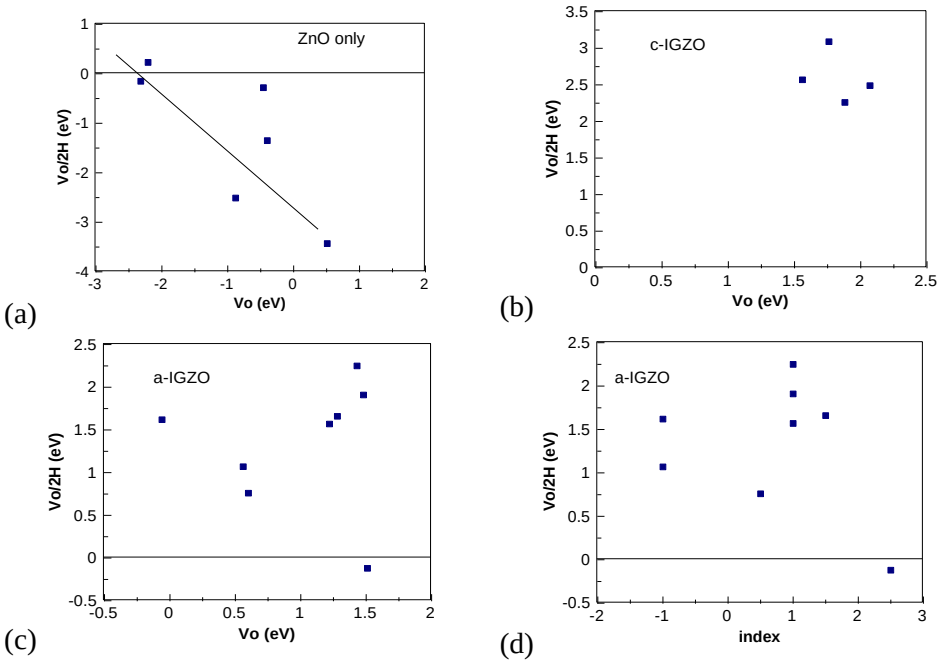

Fig. 12. Correlation of defect formation energies of Vo and Vo/2H in (a) c-ZnO, (b) c-IGZO and (c) a-IGZO. (d) Defect formation energy for Vo/2H vs bonding index for a-IGZO.

Fig 12(a) shows the correlation between the formation energy of the O vacancy and of the V_O/2H complex for a-ZnO, both in the O-poor limit, using data from Table 2. Although the two formation energies are weakly correlated, it shows that the V_O/2H complex tends to become less stable as the basic V_O becomes more stable. Thus less stable O vacancies bind 2H more strongly. Fig 12(b,c) shows a similar plot for formation energies of Vo/2H vs Vo for c-IGZO and a-IGZO, using data from Tables 3 and 4, respectively. For a-IGZO there is no clear trend. Fig 12(d) shows the V_O/2H formation energy plotted against the compositional index of Table 3.

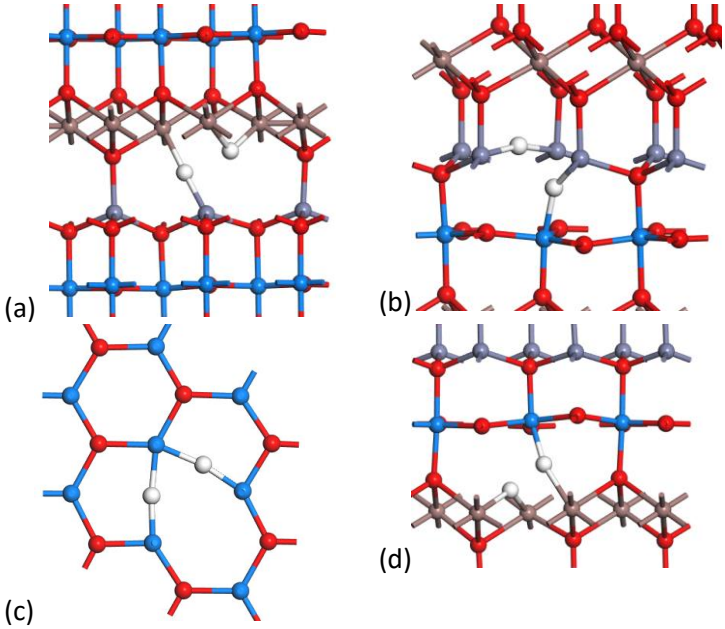

Fig. 13. Different O vacancy configurations in c-IGZO: blue=Ga, brown=In, grey=Zn, red=O.

Fig 13 shows the stable configurations of two hydrogens at the four various O vacancies in c-IGZO shown previously in Fig 5. Fig 12(d) shows the Vo/2H defect formation energy for different defects vs bonding index, and that the most stable complex occurs for the vacancy with mostly Zn neighbors. This may be because it satisfies valence best, rather than having the strongest bonds.

From this data, we can now plot the average defect formation vs Fermi energy for various charge states for the O vacancy with different hydrogen contents in c-IGZO as in Fig 14(a). This shows that the neutral V_O/2H is 2.5 eV endothermic in the O-poor limit, and that the H^+ interstitial is more stable than the 0 or +2 charged complex. This is the same situation as in c-ZnO [33]. The large formation energy means that there will not be a large concentration of 2H defects formed in c-IGZO. It also means that the hydrogens tend to be isolated and act as donors, as the H^+ energy is lower over a significant range of Fermi energies.

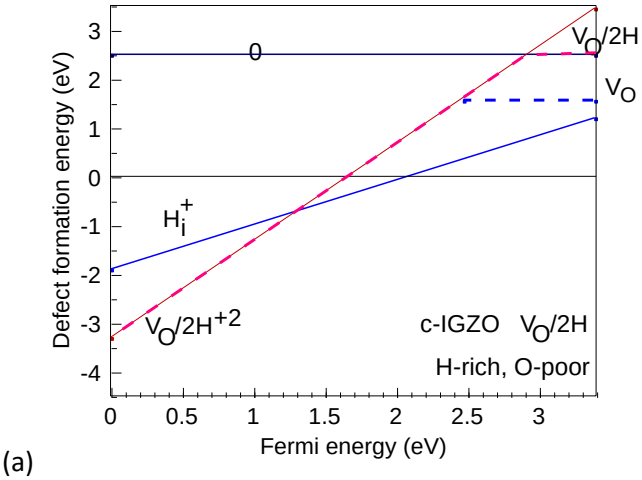

(a)

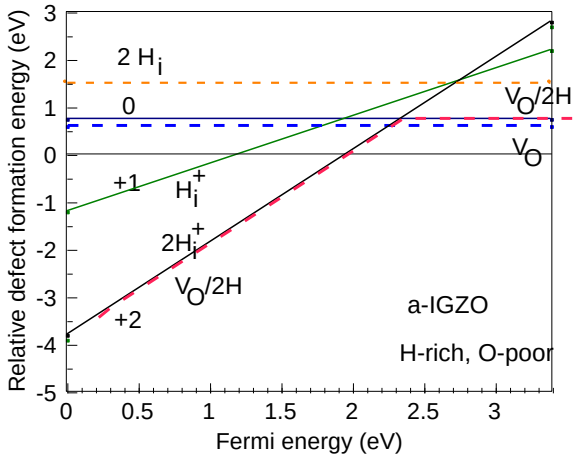

(b)

Fig. 14. Defect formation energy v. Fermi energy for hydrogen states at O vacancies in different charge states in IGZO. (a) crystal, (b) amorphous. Note that in the crystal, the V/2H complex passes through charge states +2, +1 and 0 configuration sequentially as E_F is raised, whereas in amorphous IGZO it goes from +2 to 0 directly. Also, the neutral Vo/2H complex has much lower formation energy (by 0.7 eV) which explains the much higher H content of the amorphous phase.

This behavior can be compared with that of average defect formation vs Fermi energy for the O vacancy and hydrogenated complex in *amorphous* IGZO as given in Fig 14(b). First, we see that the vacancy formation energy is lower in a-IGZO than in the crystal. This is because of the smaller density of a-InGaZnO, which allows the O vacancy to relax more and lower its energy. The effect is not quite as large as in a-ZnO but it still occurs. Next, the hydrogens enter the vacancy and form two bridge bonds. There is an energy gain for the two interstitial H_i sites in forming the bridge bonds. In contrast to the situation for the crystal, the stable configuration for H in a-IGZO is either neutral

V_O/2H or V_O^{2+}/H_2 (red line). The H_i^+ state (green line) always has a higher energy. Thus, the paired compensated configuration always has lower energy than the isolated interstitial doping configuration.

The formation energy of V_O/2H is relatively small. This means that at typical deposition temperatures of 250 - 300C there will be significant concentrations of this defect in a-IGZO. The PDOS calculations in Fig 10(b) find that this defect gives rise to a filled defect state band just above the valence band edge at +0.6 eV. This is slightly closer to the VB top than in a-ZnO. This the defect band seen in hard XPS [11,12]. As noted earlier, the vibrational signature of the Zn-H-Zn bridge bonds at 1400 cm^{-1} and 1520 cm^{-1} are seen in the IR spectra [35]. This mode frequency depends mostly on the hydrogen site being two-fold coordinated and the hydrogen bond angle, and little on the species of the metal involved, due to the light mass of the hydrogen.

The formation energy vs Fermi energy behavior shown in Fig. 14(b) with the +1 state being always above the 0 and +2 states is that of a negative U defect. Thus, this defect complex shares this property with the basic O vacancy defect [43,44]. Therefore the vacancy/ 2 H complex will also have a recombination barrier to photo-excited defects, consistent with a persistent photoconductivity [10].

Finally, Fig 15(a) shows two bridging metal-H-metal units in an amorphous IGZO network. The metal atoms involved in the bridges are shown in dark color. Fig 15(b) shows a typical a-ZnO network containing a mixture of Zn-H-Zn brdge units and hydrogens bonded to oxygen atoms. As there are two of the latter sites, overall this network has E_F in midgap.

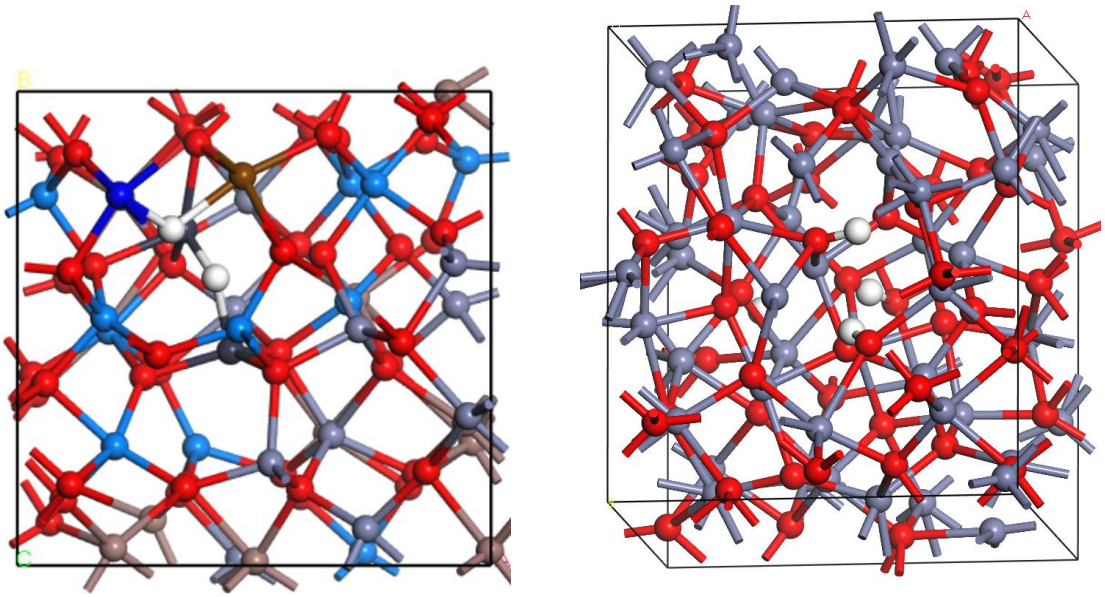

Fig. 15(a). Random network of InGaZn oxide with a neutral 2H unit at an O vacancy, forming two metal-H-metal bridge units. Darker balls are the atoms in the bridge units. (b) typical a-ZnO network with hydrogen atoms in different configurations.

Discussion

The above model accounts for the NBIS effect. It gives rise to filled defect states in the lower band gap that can be photo-excited. The Vo/2H defect complex has a negative U so it has a barrier to recombination. It corresponds to an oxygen deficiency, which is consistent with the instability being lessened by oxygen plasma or high pressure O_2 treatments [15,16]. On the other hand, hydrogen has a beneficial effect in IGZO in passivating defects [27,31,67].

The formation energy of the defect complex is on average less than 1 eV in the amorphous phase, which explains its high concentration in as deposited films, which are seen in hydrogen desorption experiments [35]. The preference for the 2H or 0H configuration explains why the compensated phase is energetically preferred.

It is interesting to compare the behavior of H in IGZO with its behavior in a-Si:H. Hydrogen is introduced into a-Si to passivated the Si dangling bonds, and so reduce the gap state density.

Hydrogen is also thought to insert into weak Si-Si bonds and thereby sharpen up the tail state distribution [68,69].

There are some similarities between the behavior of H in IGZO and in a-Si:H. However, IGZO has many differences to a-Si:H. The conduction band of a-IGZO many fewer tail states than a-Si:H [4]. The main effect of this is that we can easily move E_F above the conduction band mobility edge into the extended states by field effect or doping [4]. This differs from a-Si:H. Here, the localization of tail states is greater, their density is much greater, and they have more directional p-state character [1].

In a-Si:H the dopants undergo a rearrangement process, that pins E_F below the mobility edge [70,71], and thus doping is unable move E_F into the extended states.

Now, interstitial hydrogen is a shallow donor in ZnO [36] and in a-IGZO. Why can the hydrogen sometimes lead to high levels of doping, and in other cases to no doping? The difference is that the normal donors in ZnO or IGZO all have s-like orbital character, so they do not undergo these reactions. On the other hand, once an O vacancy has been formed, its sp^3 hybrids are directional with p-like character as in a-Si:H, and are highly localized, especially when reacting with two hydrogens. Thus, the network undergoes the Anderson negative U reaction to produce a zero density of states at E_F by an electron-lattice coupling [72], and give rise to a compensated structure. The process is enabled by the closeness of the O chemical potential of water/hydrogen to that of the metal oxides.

Finally, we previously discussed the behavior and dissociation of water in a-ZnO [33]. It should be noted that experimentally, water sometimes only partially dissociates on ZnO surfaces [73], and this may also occur on internal surfaces in lower density a-ZnO or a-IGZO.

Summary

We have carried out comprehensive density functional calculations on the oxygen vacancy and hydrogen defects in a-ZnO and in amorphous InGaZn oxide. These have been used to understand the origins of the negative bias illumination stress instability. The hydrogen pair trapped at an oxygen vacancy is found to be the defect that satisfies most of the conditions required, it is oxygen deficient, it has a negative U which creates the energy barrier to recombination and a persistent photoconductivtiy, it gives gap states just above the valence band edge and it has the vibration signature consistent with the NBIS effect.

Acknowledgements
The authors acknowledge funding from EPSRC grants EP/P005152/1.

References

1. H Hosono, J Non Cryst Solids 203 334 (1996); 352 851 (2006)
2. T Kamiya, H Hosono, NPG Asia Mater 2 15 (2010)
3. J Robertson, Phys Stat Solidi B 245 1026 (2008)
4. J Robertson, J Non-Cryst Solids 358 2437 (2012)
5. K. Ghaffarzadeh, A. Nathan, J. Robertson, S. Kim, S. Jeong, C. Kim, U. Chung, and J. Lee, Appl. Phys. Lett. **97**, 113504 (2010); Appl. Phys. Lett. **97**, 143510 (2010)
6. D H Lee, K Kawamura, K Nomura, T Kamiya, H Hosono, Electrochem Solid State Lett 13 H324 (2010)
7. M D H Chowdhury, P Miliorato, J Jang, App Phys Lett 97 173506 (2010)
8. J K Jeong, J Mater Res 28 2071 (2013)
9. J S Park, W J Maeng, H S Kim, J S Park, Thin Solid Films 520 1679 (2012)
10. S Jeon, S E Ahn, I Song, Ckim, U I Chung, E H Lee, I Yoo, A Nathan, S Lee, J Robertson, K Kim, Nature Mat 11 301 (2012)
11. K Nomura, T Kamiya, E Yanagi, E Ikenaga, K Yang, K Kobayashi, M Hirano, H Hosono, App Phys Lett 92 202117 (2008)
12. K Nomura, T Kamiya, E Ikenaga, H Yanagi, K Kobayashi, H Hosono, J App Phys 109 073726 (2011)
13. B Ryu, H K Noh, E A Choi, K N Chang, App Phys Lett 97 022108 (2010)
14. H K Noh, K J Chang, B Ryu, W J Lee, Phys Rev B 84 1115205 (2011)
15. G Um, M Mativenga, J Jang, App Phys Lett 103 033501 (2013)
16. K H Ji, J I Kim, H Y Jung, S Y Park, R Choi, U K Kim, C S Hwang, D Lee, H Hwang, J K Jeong, App Phys Lett 98 103509 (2011)
17. S Yang, K H Ji, U K Kim, C S Hwang, S H Park, C S Hwang, J Jang, J K Jeong, App Phys Lett 99 102103 (2011)
18. S Lany, A Zunger, Phys. Rev. B **72,** 035215 (2005)
19. A Janotti, C G Van de Walle, Appl. Phys. Lett. **87,** 122102 (2005)
20. H M Nahm, Y S Kim, D H Kim, Phys Stat Solidi B 249 1277 (2012)
21. J Robertson, Y Guo, App Phys Lett 104 162102 (2014)
22. W Korner, D F Urban, C Elsasser, J App Phys 114 163704 (2013)
23. A Walsh, J L F DaSilva, S H Wei, Chem Materials 21 5119 (2009)
24. S Sallis, K T Butler, N F Quackenbush, D S Williams, M Junda, D A Fischer, J C Woicik, N J Podraza, B E White, A Walsh, L J F Piper, App Phys Lett 104 232108 (2014)
25. H H Nahm, C H Park, Y S Kim, Sci Reports 4 4124 (2014)
26. Y Kang, B D Ahn, J H Song, Y G Mo, H H Nahm, S Han, J K Jeong, Adv Electronic Mats 1 1400006 (2015)
27. K Nomura,T Kamiya, H Ohta, M Hirano, H Hosono, App Phys Lett 93 192107 (2008)
28. T Kim, Y Nam, J Hur, S H K Park, S Jeon, Electron Device Letts 37 1131 (2016)
29. K Nomura, T Kamiya, H Hosono, ECS J Solid State Sci Technol 2 5 (2013)
30. Y Hanyu, K Domen, K Nomura, H Hiramatsu, H Kumomi, H Hosono, T Kamiya, App Phys Lett 103 202114 (2013)
31. T Miyase, K Watanabe, I Sakaguchi, N Ohashi, K Domen, K Nomura, H Hiramatsu, H Kumomi, H Hosono, T Kamiya, ECS Solid State Sci Technol 3 Q3085 (2014)
32. H Tang, Y Kishida, K Ide, Y Toda, H Hiramatsu, S Matsuishi, S Ueda, N Ohashi, H Kumomi, H Hosono, T Kamiya, ECS J Solid State Sci Technol 6 P365 (2017)
33. H Li, Y Guo, J Robertson, Sci Rep 7 16858 (2017)
34. M H Du, K Biswas, Phys Rev Lett 106 115502 (2011)
35. J Bang, S Matsuishi, H Hosono, App Phys Lett 110 232105 (2017)
36. C G van de Walle, Phys Rev Lett 85 1012 (2000)
37. M G Wardle, J P Goss, P Briddon, Phys Rev Lett 96 205504 (2006)
38. G A Shi, M Saboktakin, M Stavola, S J Pearton, App Phys Lett 85 5601 (2004)
39. A Janotti, C G van de Walle, Nature Mater 6 44 (2007)
40. E V Lavrov, F Herklotz, J Weber, Phys Rev Lett 102 185502 (2009)
41. K Ellmer, A Bikowski, J Phys D 49 413002 (2016)
42. S. J. Clark, M.D. Segall, C.J. Pickard, P. J. Hasnip, M. J. Probert, K. Refson, M.C. Payne, Kristallogr 220, 567 (2005)
43. A Janotti, D Segev, C G van de Walle, Phys Rev B 74 045202 (2006)
44. S Lany, A Zunger, Phys Rev Lett **98** 045501 (2007);
45. S Lany, A Zunger, Phys Rev B 80 085202 (2009)
46. P Agoston, K Albe, R M Nieminen, M J Puska, Phys Rev Lett 103 245501 (2009)
47. S J Clark, J Robertson, Phys Rev B 82 085208 (2010)
48. J Heyd, G E Scuseria, M Ernzerhof, J Chem Phys 118 8207 (2003)

49. F Oba, A Togo, I Tanaka, J Paier, G Kresse, Phys Rev B **77** 245202 (2008)
50. S J Clark, J Robertson, S Lany, A Zunger, Phys Rev B 81 115311 (2010)
51. S Lany, A Zunger, Phys Rev B 78 235104 (2008)
52. K H Lin, S Y Sun, S P Ju, J Y Tsai, H T Chen, J Y Hsieh, J App Phys 113 073512 (2013)
53. A Pandey, H Scherich, D A Drabold, J Non-Cryst Solids 455 98 (2017)
54. E P O'Reilly, J Robertson, Phys Rev B 34 8684 (1986)
55. E Fois, A Selloni, G Pastore, Q M Zhang, R Car, Phys Rev B 45 13378 (1992)
56. B Cai, D A Drabold, Phys Rev B 84 075216 (2011)
57. D McCulloch, D R McKenzie, C Goringe, J App Phys 88 5028 (2000)
58. H Omura, H Kumomi, K Nomura, T Kamiya, M Hirano, H Hosono, J Appl Phys 105 093712 (2009)
59. K Nomura, T Kamiya, H Ohta, T Uruga, M Hirano, H Hosono, Phys Rev B 75 035212 (2007)
60. T Kamiya, K Nomura, H Hosono, Phys Stat Solidi A 206 860 (2009)
61. M Nespolo, A Sato, T Osawa, H Ohashi, Cryst Res Technol 35 151 (2000)
62. K Ide, M Kikuchi, M Sasase, H Hiramatsu, H Kumomi, H Hosono, T Kamiya, AM-FPD (IEEE, 2016) p7-2; Jpn J App Phys 56 03BB03 (2017)
63. A Murat, A U Adler, T O Mason, J E Medvedeva, J Amer Chem Soc 135 5685 (2013)
64. M D Pashley, Phys Rev B 40 10481 (1989)
65. L Lin, J Robertson, App Phys Lett 98 082903 (2011)
66. A Kobayashi, O F Sankey, J D Dow, Phys Rev B 28 946 (1983)
67. T Kim, Y Nam, J Hur, S H K Park,S Jeon, Electron Device Letts 37 1131 (2016)
68. K Winer, L Ley, Phys Rev B 36 6072 (1987);
69. K Weiner, I Hirabayashi, L Ley, Phys Rev B 38 7680 (1988)
70. R A Street, Phys Rev Lett 49 1187 (1982)
71. J Robertson, J Phys C 17 L349 (1984)
72. P W Anderson, Phys Rev Lett 34 953 (1974)
73. B Meyer, D Marx, O Dulub, U Diebold, M Kunat, D Langenberg, C Woll, Angew Chem Int Ed 43 6641 (2004); O Dulub, B Meyer, U Diebold, Phys Rev Lett 95 136101 (2005)